Available online at www.sciencedirect.com
SCIENCE DIRECT®
Journal of Catalysis 220 (2003) 84–91
JOURNAL OF CATALYSIS
www.elsevier.com/locate/jcat

Density functional theory study of benzene oxidation over Fe-ZSM-5

Jason A. Ryder,[a] Arup K. Chakraborty,[a,b] and Alexis T. Bell [b,*]

[a] *Department of Chemical Engineering, University of California at Berkeley, Berkeley, CA 94720-1462, USA*
[b] *Department of Chemistry, University of California at Berkeley, Berkeley, CA 94720-1462, USA*

Received 10 February 2003; revised 29 May 2003; accepted 11 June 2003

Abstract

In the presence of nitrous oxide, Fe-ZSM-5 is known to catalyze the partial oxidation of benzene to phenol with high selectivity. The active site for this reaction is thought to be a surface iron–oxo species generated upon dissociation of nitrous oxide and release of nitrogen. In this study, density functional theory calculations were used to explore possible pathways for benzene oxidation at an isolated Fe center in ZSM-5. $Z^-[FeO_2]^+$ and $Z^-[FeO]^+$ were considered as candidate active centers. The most favorable pathway involves the direct oxidation of benzene via the reaction $Z^-[FeO_2]^+(C_6H_6) \rightarrow Z^-[FeO]^+(C_6H_5OH)$. Consistent with experimental observations, we predict that the kinetic isotope effect for the oxidation of 1,3,5-d_3-benzene is near unity at 298 K. An overall mechanism for N_2O oxidation of benzene to phenol is proposed on the basis of an analysis of relative rates of N_2O decomposition and benzene oxidation. In the case of the isolated active center $Z^-[FeO_2]^+$, the system shows a clear preference for benzene oxidation, whereas nitrous oxide dissociation is favored over $Z^-[FeO]^+$. This mechanism is then used to derive an expression for the overall rate of benzene oxidation. The apparent activation energy deduced from this rate expression ranges from 37 to 27 kcal/mol over the temperature range 600 to 800 K. At 673 K, the predicted turnover frequency compares well with that measured experimentally.

Keywords: Benzene oxidation; Fe-ZSM-5; Density functional theory

1. Introduction

The direct oxidation of benzene to phenol is an attractive alternative to the traditional cumene process, which co-produces acetone as a by-product. Studies by Panov and co-workers [1–6] have shown that nearly 100% selectivity to phenol can be achieved by oxidizing benzene with N_2O over ZSM-5 containing extra-framework iron. These findings have stimulated an interest in identifying the nature of the active site for the hydroxylation of benzene and the mechanism via which the reaction occurs. Brønsted acid sites [7–9], extra-framework iron–oxo species [1–6], and Lewis acidic aluminum sites in both framework and extra-framework positions [10,11] have been proposed as candidates for the catalytically active centers. Recent experimental studies by Wichterlova and co-workers [12] strongly support the original evidence of Panov and co-workers that extra-framework iron–oxo species are essential for the hydroxylation of benzene. A correlation in activity for phenol formation was found with the concentration of Fe in the zeolite, but not with the concentration of Brønsted or Al–Lewis sites. While the exact structure of the active center was not defined, it was suggested that it is a complex oxo-structure containing iron as Fe(III).

Several quantum chemical studies have been reported aimed at further defining the possible structure of the iron–oxo site. These efforts have focused on both the processes involved in the decomposition of N_2O and those involved in the oxidation of benzene to phenol. Zhidomirov and co-workers [13] have reported calculations for the decomposition of N_2O on an active site modeled as $Fe(OH)_2(H_2O)_2$. In a subsequent study, these authors investigated the decomposition of N_2O on binuclear Fe complexes in ZSM-5 [14]. The zeolite was modeled by a pair of 5T rings sharing an edge and the Fe complex was represented as either $[(OH)FeOFe(OH)]^{2+}$ or $[FeOFe]^{2+}$. More recently, Ryder et al. [15] have shown that N_2O decomposition to N_2 and O_2 could occur on isolated sites, i.e., $[FeO]^+$ and $[FeO_2]^+$, and that the apparent activation energy determined from an analysis of the reaction kinetics is in very good agreement with that measured experimentally [16]. Yoshizawa et al. [17–20] have considered the oxidation of benzene assuming that the active center is $[FeO]^+$. The zeolite is repre-

* Corresponding author.
E-mail address: bell@cchem.berkeley.edu (A.T. Bell).

0021-9517/$ – see front matter
doi:10.1016/S0021-9517(03)00275-6

sented by a 3T cluster, which is fully relaxed during the calculations. The authors conclude that adsorbed benzene reacts via a two-step mechanism. In the first step, benzene dissociates to form a phenyl group and a hydroxyl group. The phenyl group then migrates to the hydroxyl group and reacts with it, and the product, phenol, then desorbs. The principle issue with this mechanism is that requires Fe(III) to be reduced to Fe(I), which does not seem plausible.

The purpose of this study is to explore the energetics of benzene oxidation over both $[FeO]^+$ and $[FeO_2]^+$, using a 5T cluster representation of the zeolite framework. We proceed by postulating a general mechanism for the oxidation of benzene, computing the energetics for each elementary step, and then developing a rate expression for the overall rate of reaction, which includes the decomposition of N_2O to produce N_2 and the active form of oxygen. The apparent activation energy and turnover frequency determined from the overall rate expression are compared with experimental observation.

2. Theoretical methods

The catalytically active center and a portion of the zeolite framework are represented by a 24-atom cluster. As shown in Fig. 1, the portion of the cluster describing the zeolite contains an Al atom in the T12 site of the framework surrounded by shells of O and Si atoms. The terminal Si atoms are fixed in their crystallographic positions as reported by Olson et al. [21]. Dangling bonds are terminated by H atoms located 1.5 Å from each terminal Si atom oriented in the direction of the next T (tetrahedral) site. The anionic cluster is charge-compensated by a metal–oxo species, $[FeO]^+$ or $[FeO_2]^+$, placed between two of the four O atoms surrounding the Al atom.

Quantum chemical calculations of the geometry and energies of ground states and transition-state structures were performed using nonlocal, gradient-corrected density-functional theory [22]. To represent the effects of exchange and correlation, Becke's three-parameter exchange functional and the correlation functional of Lee, Yang, and Parr (B3LYP) were used [23,24]. Basis sets at the 6-31G or double-ζ level were used for all atoms, with the exception of Fe. To describe Fe, the energy-consistent pseudopotentials of Stuttgart and Bonn were used in the small-core approximation [25]. Polarization functions were added to all atoms, with the exception of terminal H groups. No corrections were made for basis-set superposition error. All calculations and reported values were carried out using the JAGUAR 4.1 suite of programs (Schrödinger Inc.) [26]. For purposes of comparison, additional calculations were performed using GAUSSIAN 98 [27]. During these calculations all atoms of the cluster were allowed to relax with the exception of the terminal Si and H atoms, as noted above.

Overall equilibrium constants and reaction rate constants were computed using standard statistical mechanics and absolute rate theory [28]. We use the harmonic approximation and included the contributions of the translational, rotational, and vibrational partition functions of all gaseous species participating in the reaction and the vibrational contribution due to the zeolite cluster. Since the zeolite cluster

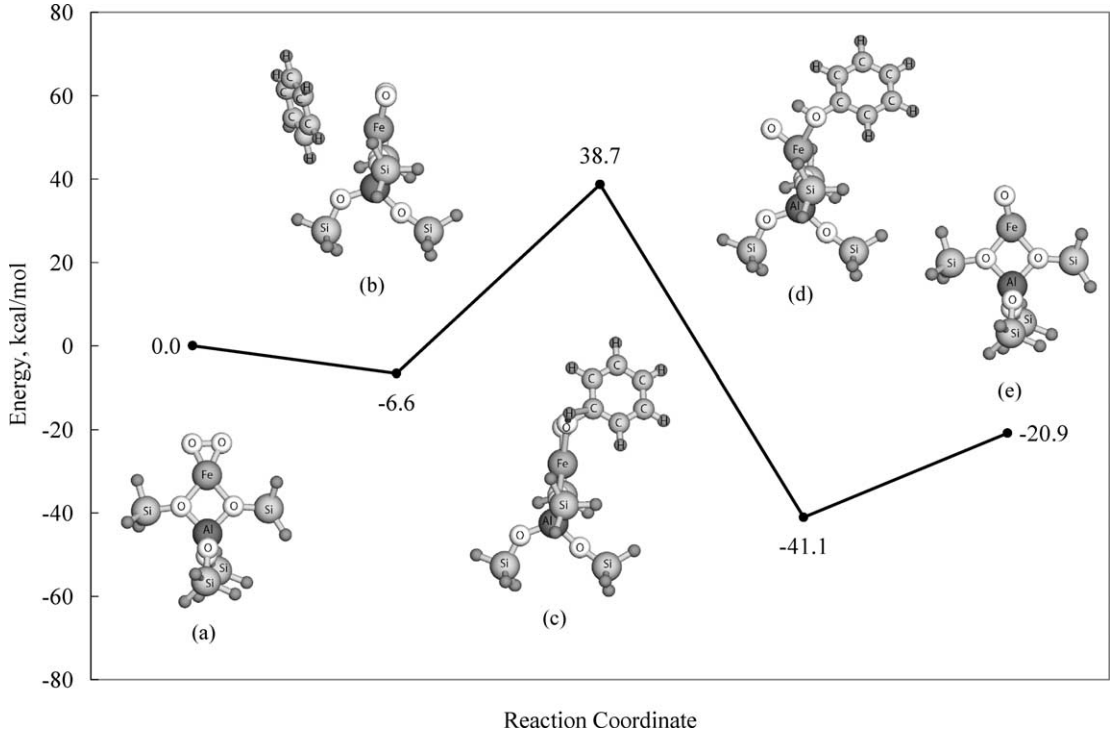

Fig. 1. Energy versus reaction coordinate for benzene oxidation over $Z^-[FeO_2]^+$.

is part of a solid, translational partition, functions for the zeolite were assumed to be equal in the reactant and transition state. For weakly bound species, contributions of restricted rotation were considered. All molecular structures were assumed to be in the ground-state electronic configuration.

3. Results and discussion

Prior to examining the energetics of benzene oxidation by N_2O, it is useful to briefly review the results of our earlier work on the decomposition of N_2O over Fe-ZSM-5 [15]. The following five steps were found to give a good representation of the mechanism:

(1) $Z^-[FeO]^+ + N_2O(g) \rightleftharpoons Z^-[FeO]^+(N_2O)$;
(2) $Z^-[FeO]^+(N_2O) \rightarrow Z^-[FeO_2]^+ + N_2$ (g);
(3) $Z^-[FeO_2]^+ + N_2O$ (g) $\rightleftharpoons Z^-[FeO_2]^+(N_2O)$;
(4) $Z^-[FeO_2]^+(N_2O) \rightarrow Z^-[FeO]^+(O_2) + N_2$ (g);
(5) $Z^-[FeO]^+(O_2) \rightarrow Z^-[FeO]^+ + O_2$ (g).

The equilibrium constants for those steps found to be at quasi-equilibrium and rate coefficients for the steps found to be irreversible are listed in Table 3. From a detailed analysis of the kinetic mechanism, we concluded that the most abundant surface species is $Z^-[FeO_2]^+$. Recent X-ray absorption spectroscopy studies support this conclusion [29].

Since $Z^-[FeO_2]^+$ is the predominant species present on the catalyst surface during N_2O decomposition, we first considered the possibility that this species participates in the oxidation of benzene in the following manner:

(6) $Z^-[FeO_2]^+ + C_6H_6$ (g) $\rightleftharpoons Z^-[FeO_2]^+(C_6H_6)$;
(7) $Z^-[FeO_2]^+(C_6H_6) \rightarrow Z^-[FeO]^+(C_6H_5OH)$;
(8) $Z^-[FeO]^+(C_6H_5OH) \rightleftharpoons Z^-[FeO]^+ + C_6H_5OH$ (g).

Reaction (6) involves the reversible adsorption of benzene, whereas reaction (7) describes the oxidation of benzene to phenol. The desorption of phenol is described by reaction (8). Fig. 1 represents the energetics for reactions (6)–(8). Structures (a) and (b) represent minimum energy structures and (c) represents the transition state for reaction (7) (Fig. 1). At each point along the reaction coordinate, the sextet (total spin $5/2$) potential energy surface lies below those of the doublet (total spin $1/2$) and quartet (total spin $3/2$) for Fe.

The energy of benzene absorption, ΔE_{ads}, is defined as the difference in energy between (a) and (b) and is computed to be -6.6 kcal/mol. The activation energy for benzene oxidation, E_{act}, is defined as the difference in energy between the adsorbed (b) and the transition state (c). This value, corrected for zero-point energy, is 41.9 kcal/mol. The imaginary frequency associated with the transition-state mode is $1219i$ cm^{-1}. The desorption energy for phenol, ΔE_{des}, defined as the difference in energy between (d) and (e), is computed to be $+20.2$ kcal/mol.

Table 1 summarizes the bond lengths for species present along the reaction pathway shown in Fig. 1. In this table, the C and O atoms involved in a reaction are identified by an asterisk. The distance between the two O atoms in $Z^-[Fe(O)_2]^+$ is 0.135 nm and the Fe–O bond distance is 0.196 nm. Both distances are typical of peroxide species. Formation of the transition state leading to phenol involves a lengthening of the O–O* bond in $Z^-[Fe(O)_2]^+$ to 0.268 nm at the same time that O* begins to form a C*–O* and an O*–H bond with benzene. The lengths of these bonds in the transition state are 0.141 and 0.144 nm, respectively. Passage from the transition state to the product state leads to a further lengthening of the O–O* bond length to 0.271 nm. At the same time, the C*–O* bond remains nearly the same as in the transition state, whereas the O*–H bond length decreases to 0.097 nm. Once phenol desorbs, the Fe–O bond length in $[FeO]^+$ decreases to 0.165 nm.

As a variant to the concerted reaction pathway represented by reactions (6)–(8), the possibility was considered that adsorbed benzene may first react to form phenoxy and hydroxyl groups and that phenol is then formed by migration of a proton to the phenoxy group. Since the barrier for the first step in this process is significantly higher than that for reaction (7), the stepwise mechanism is not considered likely.

A second possible route for partial oxidation involves the oxidation of benzene by the product of reaction (8), $Z^-[FeO]^+$,

Table 1
Selected bond lengths of equilibrium and transition-state structures for benzene oxidation over $Z^-[FeO_2]^+$

	$Z^-[FeO^*O]^+$	$\{Z^-[FeO^*O(C_6H_6)]^+\}^{2+}$	$Z^-[FeO(C_6H_5O^*H)]^+$	$Z^-[FeO]^+$
r(Fe–O) (nm)	0.196	0.209	0.220	0.165
r(Fe–O*) (nm)	0.196	0.168	0.167	
r(O*–O) (nm)	0.135	0.268	0.271	
r(C*–O*) (nm)		0.141	0.140	0.139[b]
r(O*–H) (nm)		0.144	0.097	0.097[b]
r(C*–H) (nm)	0.109[a]	0.120	0.197	

* Denotes carbon and oxygen atoms involved in bond breakage and formation.
[a] C*–H bond length in gas-phase C_6H_6.
[b] O*–H and C*–H bond lengths in C_6H_5OH.

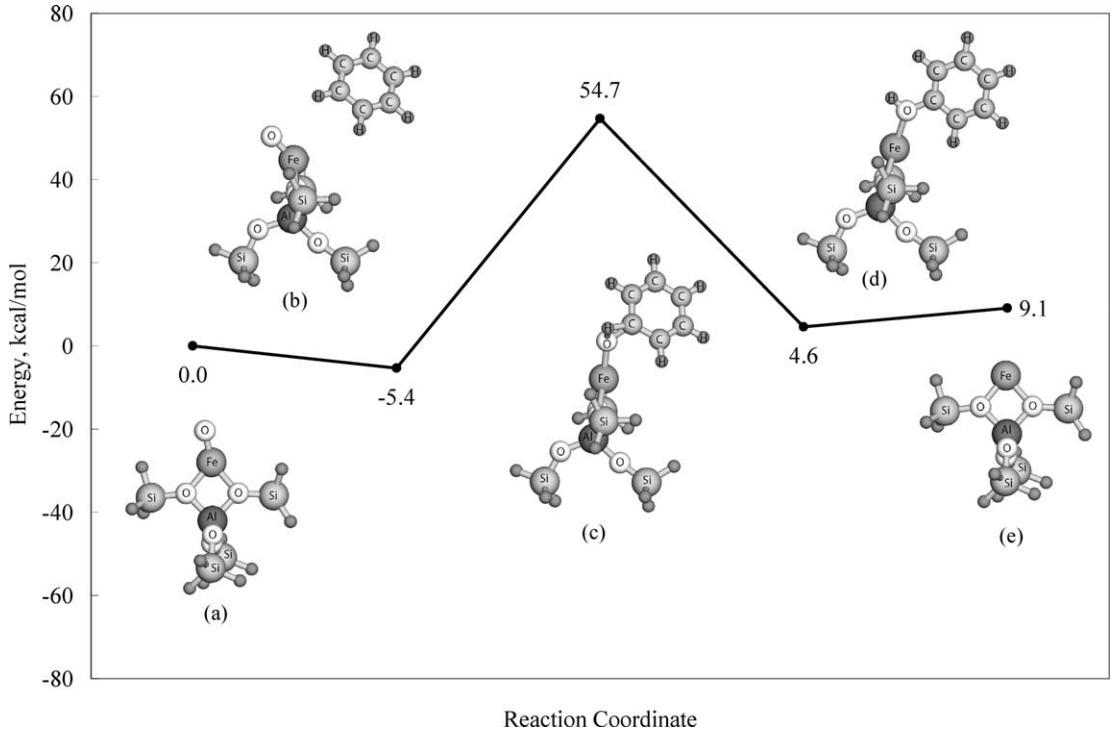

Fig. 2. Energy versus reaction coordinate for benzene oxidation over $Z^-[FeO]^+$.

Table 2
Selected bond lengths of equilibrium and transition-state structures for benzene oxidation over $Z^-[FeO]^+$

	$Z^-[FeO^*]^+$	$\{Z^-[FeO^*(C_6H_6)]^+\}^{2+}$	$Z^-[Fe(C_6H_5O^*H)]^+$	$Z^-[Fe]^+$
r(Fe–O*) (Å)	0.165	0.195	0.202	
r(C*–O*) (Å)		0.151	0.141	0.139[b]
r(O*–H) (Å)		0.124	0.097	0.097[b]
r(C*–H) (Å)	0.109[a]	0.126	0.196	

* Denotes carbon and oxygen atoms involved in bond breakage and formation.
[a] C*–H bond length in C_6H_6.
[b] O*–H and C*–H bond lengths in C_6H_5OH.

(9) $Z^-[FeO]^+ + C_6H_6\ (g) \rightleftharpoons Z^-[FeO]^+(C_6H_6)$;
(10) $Z^-[FeO]^+(C_6H_6) \rightarrow Z^-[Fe]^+(C_6H_5OH)$;
(11) $Z^-[Fe]^+(C_6H_5OH) \rightleftharpoons Z^-[Fe]^+ + C_6H_5OH\ (g)$.

Reactions (9)–(11) are equivalent to (6)–(8), with the exception that $Z^-[FeO]^+$ is now the active center.

Fig. 2 gives the energetics versus reaction coordinate for reactions (9)–(11). All structures represent minimum energy structures with the exception of 2(c), which is a transition-state structure at each point along the reaction pathway. The sextet state gives the lowest energy surface for the cluster. The energy of benzene absorption, as written in reaction (9), is computed to be −5.4 kcal/mol. The activation energy for benzene oxidation, corrected for zero-point energy, is 55.3 kcal/mol. The imaginary frequency associated with the transition-state mode is $1564i\ cm^{-1}$. The desorption energy for phenol, as written in reaction (11), is computed to be +4.5 kcal/mol.

Table 2 lists the bond lengths for species involved in the reactions shown in Fig. 2. As in Table 1, C and O atoms involved in a reaction are identified by an asterisk. Most significant in this table is the observation that the length of the Fe–O* bond in $Z^-[FeO]^+$ increases from 0.165 to 0.195 nm as O* is inserted into the C*–H bond of benzene. The length of the C*–H bond in benzene increases, correspondingly, from 0.109 to 0.126 nm, in a manner similar to that observed for the reaction of benzene with $Z^-[Fe(O)_2]^+$.

While the active center in reactions (9)–(11) is identical to that reported by Yoshizawa et al. [17–20], the manner in which the calculations are carried out, the reaction pathway, and the energetics along the reaction are different. In the work of Yoshizawa et al., the whole cluster is relaxed, whereas in the present study only the central part of the cluster is relaxed. We have shown previously that full relaxation of the cluster can lead to activation energies that are lower than those obtained for the more physically realistic constrained cluster [30]. In the present study, phenol is found to form via insertion of oxygen into the C–H bond of benzene. Yoshizawa et al. [17–20], on the other hand, conclude that benzene first reacts with $Z^-[FeO]^+$ to produce phenyl

Table 3
Computed rate parameters for the elementary steps involved in nitrous oxide dissociation and benzene oxidation in Fe-ZSM-5

Reaction		E^a, ΔH^b	Constant	T (K)		
		(kcal mol^{-1})		600	700	800
(1)	$Z^-[FeO]^+ + N_2O(g) \leftrightarrow Z^-[FeO]^+(N_2O)$	$\Delta H_1{}^a = -8.0$	K_1 (atm^{-1})	1.10×10^{-4}	5.25×10^{-5}	3.06×10^{-5}
(2)	$Z^-[FeO]^+(N_2O) \rightarrow Z^-[FeO_2]^+ + N_2(g)$	$E_2{}^a = 37.6$	A_2 (s^{-1})	1.51×10^{11}	1.58×10^{11}	1.64×10^{11}
			k_2 (s^{-1})	3.01×10^{-3}	2.86×10^{-1}	8.70×10^{0}
(3)	$Z^-[FeO_2]^+ + N_2O$ (g) $\leftrightarrow Z^-[FeO_2]^+(N_2O)$	$\Delta H_3{}^b = -6.3$	K_3 (atm^{-1})	2.15×10^{-4}	1.63×10^{-4}	1.41×10^{-4}
(4)	$Z^-[FeO_2]^+(N_2O) \rightarrow Z^-[FeO]^+(O_2) + N_2$ (g)	$E_4{}^a = 44.6$	A_4 (s^{-1})	8.41×10^{10}	8.62×10^{10}	8.77×10^{10}
			k_4 (s^{-1})	4.83×10^{-6}	1.04×10^{-3}	5.79×10^{-2}
(5)	$Z^-[FeO]^+(O_2) \leftrightarrow Z^-[FeO]^+ + O_2$ (g)	$\Delta H_5{}^b = 53.3$	K_5 (atm)	6.79×10^{-13}	3.63×10^{-10}	3.96×10^{-8}
(6)	$Z^-[FeO_2]^+ + C_6H_6$ (g) $\leftrightarrow Z^-[FeO_2]^+(C_6H_6)$	$\Delta H_6{}^b = -8.0$	K_6 (atm^{-1})	5.23×10^{-2}	7.77×10^{-2}	1.39×10^{-1}
(7)	$Z^-[FeO_2]^+(C_6H_6) \rightarrow Z^-[FeO]^+(C_6H_5OH)$	$E_7{}^a = 41.9$	A_7 (s^{-1})	2.39×10^{10}	2.50×10^{10}	2.60×10^{10}
			k_7 (s^{-1})	1.28×10^{-5}	2.03×10^{-3}	9.14×10^{-2}
		$E_{-7}{}^a = 75.8$	A_{-7} (s^{-1})	3.70×10^{10}	3.91×10^{10}	4.10×10^{10}
			k_{-7} (s^{-1})	8.81×10^{-18}	8.22×10^{-14}	7.84×10^{-11}
			k_7/k_{-7}	1.45×10^{12}	2.47×10^{10}	1.17×10^{9}
(8)	$Z^-[FeO]^+(C_6H_5OH) \leftrightarrow Z^-[FeO]^+ + C_6H_5OH$ (g)	$\Delta H_8{}^b = 21.6$	K_8 (atm)	7.70×10^{-2}	1.68×10^{-1}	2.01×10^{-1}
(9)	$Z^-[FeO]^+ + C_6H_6$(g) $\leftrightarrow Z^-[FeO]^+(C_6H_6)$	$\Delta H_9{}^b = -6.8$	K_9 (atm^{-1})	1.94×10^{-3}	2.61×10^{-3}	4.18×10^{-3}
(10)	$Z^-[FeO]^+(C_6H_6) \rightarrow Z^-[Fe]^+(C_6H_5OH)$	$E_{10}{}^a = 55.3$	A_{10} (s^{-1})	1.52×10^{11}	1.69×10^{11}	1.84×10^{11}
			k_{10} (s^{-1})	1.13×10^{-9}	9.45×10^{-7}	1.48×10^{-4}
		$E_{-10}{}^a = 67.8$	A_{-10} (s^{-1})	3.58×10^{11}	4.20×10^{11}	4.80×10^{11}
			k_{-10} (s^{-1})	7.14×10^{-14}	2.83×10^{-10}	1.43×10^{-7}
			k_{10}/k_{-10}	1.59×10^{4}	3.34×10^{3}	1.03×10^{3}
(11)	$Z^-[Fe]^+(C_6H_5OH) \leftrightarrow Z^-[Fe]^+ + C_6H_5OH$ (g)	$\Delta H_{11}{}^b = 6.0$	K_{11} (atm)	6.89×10^{5}	3.06×10^{5}	1.16×10^{5}

[a] Calculated activation energy including zero-point energy correction.
[b] Calculated enthalpy averaged over 600–800 K.

and hydroxyl groups, which react further to form phenol. A further difference is that while we find the sextet to provide the lowest energy surface, Yoshizawa et al. report that the synthesis of phenol occurs with the cluster in the quartet state.

The apparent rate coefficients for benzene oxidation can be determined from analysis of reactions (6)–(8) and (9)–(11), respectively. The rate of benzene oxidation at $Z^-[FeO_2]^+$ is given by reaction (7):

$$-r^{[FeO_2]}|_{Bz} = k_7\big[Z^-[FeO_2]^+(C_6H_6)\big]. \tag{1}$$

If we assume that Step (6) is quasi-equilibrated because of the weak binding of C_6H_6, we can write

$$\big[Z^-[FeO_2]^+(C_6H_6)\big] = K_6[C_6H_6]\big[Z^-[FeO_2]^+\big]. \tag{2}$$

Thus, the rate of benzene oxidation can be expressed as

$$-r^{[FeO_2]}|_{Bz} = k_7K_6[C_6H_6]\big[Z^-[FeO_2]^+\big],$$
$$-r^{[FeO_2]}|_{Bz} = k_a^{[FeO_2]}|_{Bz}[C_6H_6], \tag{3}$$

where $k_a^{[FeO_2]}|_{Bz} = k_7K_6[Z^-[FeO_2]^+]$. The apparent activation energy, $E_a^{[FeO_2]}|_{Bz}$, is then defined as

$$E_a^{[FeO_2]}|_{Bz} = E_7 + \Delta H_6. \tag{4}$$

Table 4
Apparent activation energies and rate constants for nitrous oxide dissociation and benzene oxidation in Fe-ZSM-5

	E_a	T (K)		
	(kcal/mol)	600	700	800
$k_a^{[FeO]}|_{N_2O}$ (s^{-1})	31.8	5.72×10^{-6}	1.09×10^{-4}	9.96×10^{-4}
$k_a^{[FeO_2]}|_{N_2O}$ (s^{-1})	39.4	4.47×10^{-10}	5.15×10^{-8}	1.91×10^{-6}
$k_a^{[FeO]}|_{Bz}$ (s^{-1})	49.8	3.64×10^{-13}	3.87×10^{-10}	9.23×10^{-8}
$k_a^{[FeO_2]}|_{Bz}$ (s^{-1})	37.5	2.56×10^{-7}	6.06×10^{-5}	4.89×10^{-3}

A similar analysis of reactions (9)–(11) yields

$$-r^{[FeO]}|_{Bz} = k_{10}K_9[C_6H_6]\big[Z^-[FeO]^+\big],$$
$$-r^{[FeO]}|_{Bz} = k_a^{[FeO]}|_{Bz}[C_6H_6], \tag{5}$$
$$E_a^{[FeO]}|_{Bz} = E_{10} + \Delta H_9, \tag{6}$$

where $k_a^{[FeO]}|_{Bz} = k_{10}K_9[Z^-[FeO]^+]$. Values of k_a and E_a are provided in Table 4.

On a per-site basis, we can compute the relative rate of benzene oxidation involving $[FeO_2]^+$ and $[FeO]^+$,

$$\frac{-r^{[FeO_2]}|_{Bz}}{-r^{[FeO]}|_{Bz}} = \frac{k_a^{[FeO_2]}|_{Bz}}{k_a^{[FeO]}|_{Bz}}. \tag{7}$$

At $T = 600$ K, this ratio is 7.04×10^5 and at $T = 800$ K, this ratio is 5.29×10^4. Hence, we predict that the oxidation of benzene should proceed more readily over $[FeO_2]^+$ than $[FeO]^+$.

To test the validity of reaction (7) as the rate-determining step in the oxidation of benzene to phenol, we calculated the kinetic isotope effect (KIE) for the reaction of 1,3,5-d_3-benzene to produce $C_6H_2D_3OH$ versus $C_6H_3D_2OD$. Panov and co-workers [31] determined a KIE ≈ 1 at 25 °C for the reaction of 1,3,5-d_3-benzene with adsorbed oxygen formed by decomposition of N_2O over Fe-ZSM-5. The authors suggest that the absence of a pronounced kinetic isotope effect indicates that the rate-determining step in benzene oxidation does not involve the rupture of a carbon–hydrogen bond.

In the context of the analysis presented here, the rate-determining step in benzene oxidation is reaction (7). The rate constant for this reaction can be expressed as

$$k_7 = \left(\frac{k_B T}{h}\right) \frac{q^{2+}_{Z^-[FeO(C_6H_5OH)]^+,vib}}{q_{Z^-[FeO_2(C_6H_6)]^+,vib}} e^{-E_{Act}/RT}, \tag{8}$$

where k_B is Boltzman's constant, h is Planck's constant, and E_{Act} is the activation barrier including zero-point energy corrections. In Eq. (8) $q^{2+}_{Z^-[FeO(C_6H_5OH)]^+,vib}$ and $q_{Z^-[FeO_2(C_6H_6)]^+,vib}$ have been written to represent the vibrational partition function for the equilibrium and transition-state structures, respectively. In order to determine the kinetic KIE, we computed the ratio of kinetic rate constants for the formation of $C_6H_2D_3OH$ and $C_6H_3D_2OD$. Since the activation energy is unaffected by the presence of deuterium, this expression is simply the ratio of vibrational partition functions for the transition states

$$\text{KIE} = \frac{k_{7(C_6H_2D_3OH)}}{k_{7(C_6H_3D_2OD)}} = \frac{q^{2+}_{Z^-[FeO(C_6H_2D_3OH)]^+,vib}}{q^{2+}_{Z^-[FeO(C_6H_3D_2OD)]^+,vib}}. \tag{9}$$

At 25 °C, KIE = 1.02. This result is consistent with the experimental finding of KIE ≈ 1, supporting the proposed view that reaction (7) is a plausible rate-determining step in the oxidation of benzene.

The oxidation of benzene is in direct competition with the dissociation of N_2O whether the active species is $[FeO_2]^+$ or $[FeO]^+$. We can compute the relative rates of N_2O dissociation and C_6H_6 benzene oxidation for each of the two cases as follows. For the relative rate of benzene oxidation versus nitrous oxide dissociation over $[FeO_2]^+$, we write

$$\frac{-r^{[FeO_2]}|_{Bz}}{-r^{[FeO_2]}|_{N_2O}} = \frac{k_a^{[FeO_2]}|_{Bz}[C_6H_6]}{k_a^{[FeO_2]}|_{N_2O}[N_2O]}. \tag{10}$$

Similarly, for $[FeO]^+$,

$$\frac{-r^{[FeO]}|_{Bz}}{-r^{[FeO]}|_{N_2O}} = \frac{k_a^{[FeO]}|_{Bz}[C_6H_6]}{k_a^{[FeO]}|_{N_2O}[N_2O]}. \tag{11}$$

Note that $k_a^{[FeO]}|_{N_2O}$ and $k_a^{[FeO_2]}|_{N_2O}$ are the apparent rate constants for N_2O dissociation over $[FeO]^+$ and $[FeO_2]^+$, respectively, as determined in a previous publication [15] and listed in Table 4.

Table 5
Relative rates of nitrous oxide dissociation and benzene oxidation over Fe-ZSM-5

	T (K)		
	600	700	800
$r^{[FeO_2]}\|_{Bz}/r^{[FeO]}\|_{Bz}$	7.04×10^5	1.57×10^5	5.29×10^4
$r^{[FeO]}\|_{Bz}/r^{[FeO]}\|_{N_2O}$	6.37×10^{-8}	3.56×10^{-6}	9.27×10^{-5}
$r^{[FeO_2]}\|_{Bz}/r^{[FeO_2]}\|_{N_2O}$	5.73×10^2	1.18×10^3	2.56×10^3

Table 5 presents the values of ratios given in Eqs. (10) and (11) versus temperature, assuming $[C_6H_6]/[N_2O] = 1$. The ratio of the rates of benzene oxidation to N_2O dissociation over $[FeO_2]^+$ is 5.73×10^2 at $T = 600$ K and 2.56×10^3 at $T = 800$ K. The ratio of the rates of benzene oxidation to N_2O dissociation over $[FeO]^+$ is 6.37×10^{-8} at $T = 600$ K and 9.27×10^{-5} at $T = 800$ K. For $[FeO]^+$, the rate of N_2O dissociation is much higher than the rate of benzene oxidation, whereas for $[FeO_2]^+$, the rate of benzene oxidation is much higher than the rate of N_2O dissociation. This important result allows us to write a complete mechanism for the oxidation of benzene by N_2O as follows:

(1) $Z^-[FeO]^+ + N_2O\,(g) \rightleftharpoons Z^-[FeO]^+(N_2O)$;
(2) $Z^-[FeO]^+(N_2O) \rightarrow Z^-[FeO_2]^+ + N_2\,(g)$;
(6) $Z^-[FeO_2]^+ + C_6H_6(g) \rightleftharpoons Z^-[FeO_2]^+(C_6H_6)$;
(7) $Z^-[FeO_2]^+(C_6H_6) \rightarrow Z^-[FeO]^+(C_6H_5OH)$;
(8) $Z^-[FeO]^+(C_6H_5OH) \rightleftharpoons Z^-[FeO]^+ + C_6H_5OH\,(g)$.

An overall rate expression for the rate of benzene oxidation can now be developed on the basis of the above scheme. Assuming, as was done above, that reaction (6) is quasi-equilibrated the rate of benzene oxidation can be written as

$$-r^{[FeO_2]}|_{Bz} = k_7 K_6 [C_6H_6]\left[Z^-[FeO_2]^+\right]. \tag{12}$$

At steady state, the rate of N_2O decomposition must be equivalent to the rate of benzene oxidation, therefore

$$-r^{[FeO]}|_{N_2O} = -r^{[FeO_2]}|_{Bz}, \tag{13}$$

$$k_2 K_1 [N_2O]\left[Z^-[FeO]^+\right] = k_7 K_6 [C_6H_6]\left[Z^-[FeO_2]^+\right].$$

The site balance on the active centers is given by

$$[L] = \left[Z^-[FeO]^+\right] + \left[Z^-[FeO_2]^+\right] + \left[Z^-\left[FeO(C_6H_5OH)\right]^+\right], \tag{14}$$

where [L] is the total concentration of Fe sites. In writing Eq. (14), it is assumed that the coverage by adsorbed N_2O and C_6H_6 is small relative to those of other species. If we assume reaction (8) is quasi-equilibrated, we can write

$$K_8\left[Z^-\left[FeO(C_6H_5OH)\right]^+\right] = [C_6H_5OH]\left[Z^-[FeO]^+\right]. \tag{15}$$

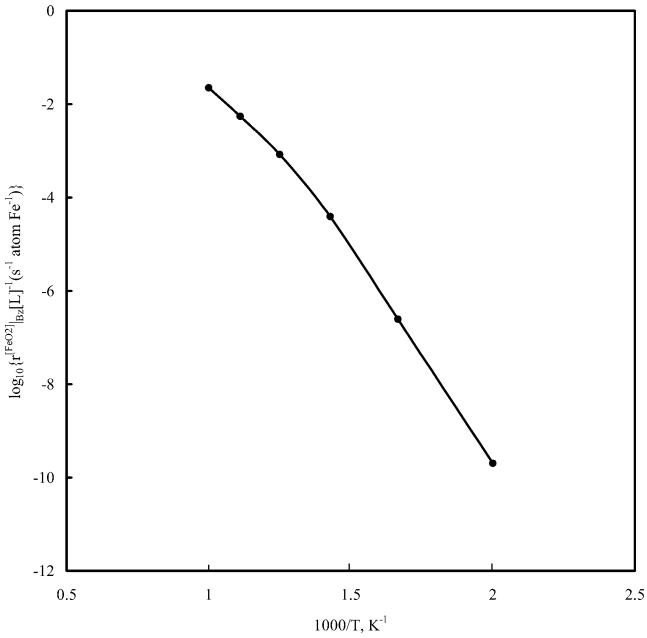

Fig. 3. Overall rate versus inverse temperature for benzene oxidation over Fe-ZSM-5.

Introducing Eq. (13) into Eq. (14) leads to the following expression for the site balance:

$$[\mathrm{L}] = \left[\mathrm{Z}^{-}[\mathrm{FeO}]^{+}\right] \times \left\{1 + \frac{k_2 K_1}{k_7 K_6}\frac{[\mathrm{N_2O}]}{[\mathrm{C_6H_6}]} + K_8[\mathrm{C_6H_5OH}]\right\}. \tag{16}$$

Then, using Eqs. (12), (13), and (16), the overall rate of benzene oxidation written as a turnover frequency is

$$\frac{r^{[\mathrm{FeO_2}]}|_{\mathrm{Bz}}}{[\mathrm{L}]} = \frac{k_2 K_1[\mathrm{N_2O}]}{\left\{1 + \frac{k_2 K_1}{k_7 K_6}\frac{[\mathrm{N_2O}]}{[\mathrm{C_6H_6}]} + K_8[\mathrm{C_6H_5OH}]\right\}}. \tag{17}$$

Note that the units of the rate are mol C_6H_6/(mol$_{Fe}$ s).

Fig. 3 shows the overall rate of benzene oxidation versus inverse temperature. For simplicity, we have assumed $[C_6H_5OH] \approx 0$ and $[N_2O]/[C_6H_6] = 1$. Note that for temperatures $\leqslant 700$ K, the apparent activation barrier for benzene oxidation, taken as the slope of $\ln\{r^{[\mathrm{FeO_2}]}|_{\mathrm{Bz}}[\mathrm{L}]^{-1}\}$ versus $1/T$, is ~ 37 kcal/mol. In this temperature regime $k_2K_1/k_7K_6 > 1$ (i.e., at $T = 600$ K, $k_2K_1/k_7K_6 = 20$) and the rate of benzene oxidation can be written as

$$\frac{r^{[\mathrm{FeO_2}]}|_{\mathrm{Bz}}}{[\mathrm{L}]} = k_7 K_6[\mathrm{C_6H_6}]. \tag{18}$$

At temperatures $\geqslant 800$ K, the apparent activation barrier is ~ 27 kcal/mol and the value of $k_2K_1/k_7K_6 < 1$ (i.e., at $T = 800$ K, $k_2K_1/k_7K_6 = 1.8 \times 10^{-2}$) and in this temperature regime the rate of benzene oxidation becomes

$$\frac{r^{[\mathrm{FeO_2}]}|_{\mathrm{Bz}}}{[\mathrm{L}]} = k_2 K_1[\mathrm{N_2O}]. \tag{19}$$

Panov and co-workers [2] have measured the conversion and selectivity of benzene oxidation by nitrous oxide over Fe-ZSM-5 for a range of temperatures (573–673 K) and iron content (0.004–0.72 wt% Fe_2O_3). Surprisingly, the authors make no mention of the measured apparent activation energy for the overall process. Our calculations based on the experimental data give values ranging from 28 to 8 kcal/mol for Fe-ZSM-5 samples containing 0.004 to 0.72 wt% Fe_2O_3, respectively. While the upper value of the range overlaps the lower value of the activation barrier reported here, no definitive conclusions can be drawn regarding the level of agreement between theory and experiment, given the wide range of values determined from the experimental results.

Reitzmann et al. [32] have recently investigated the kinetics of benzene oxidation by nitrous oxide over Fe-ZSM-5 (Si/Al = 21.5, 1.9 wt% Fe_2O_3) in a recycle reactor. At 673 K, and N_2O and C_6H_6 partial pressures of 0.03 atm, these authors report the rate of benzene consumption to be 0.05 mmol/(g_{Fe} min) and the rate of phenol formation to be 0.03 mmol/(g_{Fe} min). For these reaction conditions, our calculated rate of benzene oxidation to phenol 0.04 mmol/(g_{Fe} min), which shows very good agreement between theory and experiment. Comparison can also be made with the data of Panov et al. [2]. At 673 K, and N_2O and C_6H_6 partial pressures of 0.20 and 0.05 atm, respectively, these authors report rates of 66 to 0.9 mmol/(g_{Fe} min) for Fe-ZSM-5 containing 0.004 to 0.72 wt% Fe_2O_3. For the same conditions, Eq. (17) predicts a value of 0.1 mmol/(g_{Fe} min). In this case, the agreement between theory and experiment is not as compelling.

4. Conclusions

Two possible pathways for the N_2O oxidation of benzene over Fe-ZSM-5 have been evaluated theoretically, assuming $[FeO_2]^+$ and $[FeO]^+$ species to be the active centers. The choice of active centers was based on a previous investigation of N_2O decomposition on Fe-ZSM-5 [15]. Classical transition-state theory calculations give values of the rate of benzene oxidation that are much higher for $[FeO_2]^+$ than for $[FeO]^+$. This chemistry is further supported by the conclusion of earlier work that $[FeO_2]^+$ is the most abundant surface species in a ZSM-5 system with isolated Fe cations [15]. Both pathways compete directly with the dissociation of N_2O for active sites. The relative rates of benzene oxidation and N_2O dissociation on both $[FeO_2]^+$ and $[FeO]^+$ species have been calculated. For $[FeO]^+$, the relative rate of nitrous oxide dissociation is higher than that of benzene oxidation, whereas for $[FeO_2]^+$, benzene oxidation is preferred. The analysis presented leads to a comprehensive picture of the partial oxidation of benzene by N_2O over Fe-ZSM-5 coupled with nitrous oxide dissociation.

Acknowledgments

This work was supported by a grant from BP International, Ltd. Additional support was provided by a graduate

research fellowship from the National Science Foundation. Computational resources were provided by the National Energy Resource Supercomputer Center.

References

[1] G.I. Panov, V.I. Sobolev, A.S. Kharitonov, J. Mol. Catal. 85 (1990) 61.
[2] G.I. Panov, G.A. Sheveleva, A.S. Kharitonov, V.N. Romannikov, L.A. Vostrikova, Appl. Catal. A 82 (1992) 31.
[3] L.V. Pirutko, D.P. Ivanov, K.A. Dubkov, V.V. Terskikh, A.S. Kharitonov, G.I. Panov, in: Proceedings of the 12th International Zeolite Conference, Baltimore (1998), 1999, p. 1245.
[4] G.I. Panov, A.K. Uriarte, M.A. Rodkin, V.I. Sobolev, A.S. Kharitonov, Catal. Today 41 (1998) 365.
[5] G.I. Panov, CATTECH 4 (2000) 18.
[6] M. Iwamoto, J.I. Hirata, K. Matsukami, S. Kagawa, J. Phys. Chem. 87 (1983) 903.
[7] E. Suzuki, K. Nakashiro, Y. Ono, Chem. Lett. 211 (1988) 953.
[8] R. Burch, C. Howitt, Appl. Catal. A 103 (1993) 135.
[9] M. Gubelmann, P.J. Tirel, Patent EP 341,165, 1992.
[10] V.L. Zholobenko, I.N. Senchenya, L.M. Kustov, V.B. Kazansky, Kinet. Catal. 32 (1991) 151.
[11] L.M. Kustov, A.L. Tarasov, V.I. Bogdan, A.A. Trylov, J.W. Fulmer, Catal. Today 61 (2000) 123.
[12] P. Kubanek, B. Wichterlova, Z. Sobalik, J. Catal. 211 (2002) 109.
[13] A.L. Yakovlev, G.M. Zhidomirov, R.A. van Santen, Catal. Lett. 75 (2001) 45.
[14] A.L. Yakovlev, G.M. Zhidomirov, R.A. van Santen, J. Phys. Chem. B 105 (2001) 12297.
[15] J.A. Ryder, A.K. Chakraborty, A.T. Bell, J. Phys. Chem. B 106 (2002) 7059.
[16] B.R. Wood, J.A. Reimer, A.T. Bell, J. Catal. 209 (2002) 151.
[17] K. Yoshizawa, T. Yumura, Y. Shiota, T. Yamabe, J. Phys. Chem. B 104 (2000) 734.
[18] K. Yoshizawa, T. Yumura, Y. Shiota, T. Yamabe, Bull. Chem. Soc. Jpn. 73 (2000) 29.
[19] K. Yoshizawa, Y. Shiota, Y. Kagawa, T. Yamabe, J. Phys. Chem. A 104 (2000) 2552.
[20] K. Yoshizawa, Y. Shiota, T. Yamabe, J. Am. Chem. Soc. 121 (1999) 147.
[21] D.H. Olson, G.T. Kokotallo, S.L. Lawton, W.M. Meier, J. Phys. Chem. 85 (1981) 2238.
[22] R.G. Parr, W. Yang, Density Functional Theory of Atoms and Molecules, Oxford Univ. Press, Oxford, 1989.
[23] A.D. Becke, Phys. Rev. A 38 (1988) 3098.
[24] C. Lee, W. Yang, R.G. Parr, Phys. Rev. B 37 (1988) 785.
[25] M. Dolg, U. Wedig, H. Stoll, H. Preuss, J. Chem. Phys. 86 (1987) 866.
[26] JAGUAR 4.0, Schrödinger Inc., Portland, ME, 2000.
[27] GAUSSIAN 98, Gaussian Inc., Pittsburgh, PA, 1998.
[28] D.A. McQuarrie, Statistical Mechanics, Collins, New York, 1973.
[29] S.H. Choi, B.R. Wood, J.A. Ryder, A.T. Bell, J. Phys. Chem. B, in press.
[30] J.A. Ryder, A.K. Chakraborty, A.T. Bell, J. Phys. Chem. B 104 (2000) 6998.
[31] K.A. Dubkov, V.I. Sobolev, E.P. Talsi, M.A. Rodkin, N.H. Watkins, A.A. Shteinman, G.I. Panov, J. Mol. Catal. A 123 (1997) 155.
[32] A. Reitzmann, E. Klemm, G. Emig, Chem. Eng. J. 90 (2002) 149.